

Crack - Tip Radius Effect on Fatigue Crack Growth and Near - Tip Fields in Plastically Compressible Materials

S. Singh[#] and D. Khan^{*}

[#]*Department of Mechanical Engineering, Uttarakhand Institute of Technology,
Uttarakhand University, Dehradun - 248 007, India*

^{*}*Department of Mechanical Engineering, Indian Institute of Technology, Varanasi - 221 005, India*

**E-mail: dkhan.mec@itbhu.ac.in*

ABSTRACT

Motivated by the prospective uses of plastically compressible materials such as, metallic and polymeric foams, transformation toughened ceramics, toughened structural polymers etc., the present authors investigate the crack-tip radius effect on fatigue crack growth (FCG) of a mode I crack and near-tip stress-strain fields in such plastically compressible solids. These plastically compressible materials have been characterised by elastic-viscoplastic constitutive equations. Simulations are conducted for plane strain geometry with two different hardening functions: one is bilinear hardening and the other one is hardening-softening-hardening. It has been observed that plastic compressibility as well as strain softening lead to significant deviation in the amount of crack growth. It has further been revealed that the nature of FCG is appreciably affected by initial crack-tip radius. Even though it may look from outside that the increase in tip radius will lead to decrease in FCG, but the nature of FCG variation with respect to tip radius is found to be a combined effect of tip radius, plastic compressibility and work or strain softening etc. As to be expected when the crack-tip radius is low (smallest of the expounded variation of the present study), the rate of FCG is found to be maximum for the bilinear hardening material though the nature of FCG variation is different in plastically incompressible and compressible solids. In sharp contrast, when the material exhibits work or strain softening, the FCG rate is found to be dependent on the instantaneous crack-tip radius. For instance, as a quantitative comparison in the present study, after the end of 5th cycle, the normalised crack-tip extension for the bilinear material (plastically compressible) corresponding to the smallest tip radius is 2.9 whereas the same for the largest tip radius is 1.9. Conversely, for the material (plastically compressible) that exhibits strain softening, the corresponding tip extension values are 1.0 and 2.7 for the same smallest and largest radii, respectively.

Keywords: Finite deformation; FCG; Mode I crack; Plastic compressibility; Crack-tip radius; Strain softening

1. INTRODUCTION

Geometrical discontinuities such as holes, notches, cracks etc are unavoidable in designing engineering components and structures. These discontinuities or stress risers have been recognised to be the major locations for the behaviour estimation of such components and structures. Even if one assumes a sharp crack in the beginning of numerical computation, the crack-tip will be blunted (with highly distorted mesh) after the application of certain amount of load¹. Therefore, an initially blunted crack with a circular-arc-tip is mostly considered for numerical simulation. On the other hand, it has been reported in literature that the deformation of a crack-tip and the field quantities are much influenced by the notch tip radius and for example, only a few are mentioned here. Experiments on notched polycarbonate specimens show that failure at the notch-root is started by ductile tearing when the notch-root radius is reasonably large, however, when the notch-root radius is relatively small, and then failure starts in the form of a crack-like feature at the tip of the plastic zone around the notch²⁻³. Investigations have

also been made to explore the notch-root radius effect on the fracture toughness in ceramic materials and it has been reported that the notch-root radius could affect the toughness greatly^{4,6}. Rozumek⁷, *et al.* examined experimentally the notch tip radius effect on FCG for steel and aluminum alloy and they observed that the tip radius could influence the crack growth much. For a range of notch geometries (very sharp to a very blunt notch), Yanase and Endo⁸ investigated the notch effect in FCG for steel. While sizeable amount of literatures related to the consequence of crack-tip radius on near-tip deformation as well as fields are available for the materials mentioned above, but similar studies for plastically compressible materials such as compliant foams, plastics, transformation toughened ceramics, toughened structural polymers etc. are very insufficient even to date.

In recent times, compliant foam-like materials, for example, polymeric foams, cellular solid type foams, foams of carbon nanotubes have been in use more and more for a variety of applications owing to their high energy absorption capacity, high strength to weight ratio, highly desired electrical, thermal, acoustic as well as radiation-resistant properties. Owing to superior blast mitigation and impact

resistance of polymeric foams, they are used much as core materials in sandwich structures of aerospace and automobile industries. As metallic foam has also the capability to absorb high amount of energy before failure, it can play an important role in military applications related to armoured protection of vehicles or blast mitigation. Vertically aligned carbon nanotubes (VACNTs) are found to have prospective uses in electromechanical devices, switches and actuators where VACNTs are subjected to extensive thermomechanical stresses and strains⁹⁻¹¹. As for these foams there is volume change during the deviatoric loading, they are also known as plastically compressible materials. In the theory of classical plasticity, the role of hydrostatic pressure is neglected in plastic deformation of a material. But, for foams, yielding can occur under hydrostatic loading in addition to deviatoric loading and hence classical plasticity theory cannot be used to describe their behaviour. In numerical computation, the heterogeneous metallic foam is commonly replaced by a plastically compressible elastic-plastic/ elastic-viscoplastic material¹²⁻¹³. However, the successful application of compliant foams requires maturity in the fundamental understanding of their mechanical properties. Also, the existing computational and experimental studies related to the deformation and fracture of compliant foams have been limited mostly to compressive loading¹⁴. Therefore, looking at the potential uses of such materials in a variety of applications, it seems, developing a predictive framework for the mechanical behaviour of such materials under various kinds of loadings would be extremely useful.

The FCG is a topic of significant importance in a number of engineering applications. Although crack growth in plastically compressible materials has been studied to some extent, for example, by Singh & Khan¹⁵, many fundamentals problems are still left unresolved. One key problem is how the tip radius size influences the crack-tip plasticity and therefore the plastic crack growth under fatigue loading. The main objectives of this work are to scrutinize the role of crack-tip radius on FCG and near-tip fields for two different plastically compressible materials characterised by isotropic and rate dependent elastic- viscoplastic constitutive equations. The present computations are limited to a mode I crack with plane strain deformation, small scale yielding (SSY) and plastic normality flow rule.

2. THEORETICAL FRAMEWORK

2.1 Material Constitutive Equation

For the constitutive relation, the deformation tensor rate, d is taken to be the sum of isotropic elastic part d^e and a viscoplastic part d^p . The elastic part $d^e = L^{-1} : \hat{\tau}$ is characterised by modulus of elasticity E along with Poisson's ratio ν and we assume the elastic strains to be very small. The plastic part of the response¹⁵ is given as

$$d^p = \frac{3}{2} \frac{\dot{\epsilon}_p}{\sigma_e} p, \tag{1}$$

where,

$$p = \tau - \alpha tr(\tau)I \tag{2}$$

And

$$\dot{\epsilon}_p = \dot{\epsilon}_0 \left(\frac{\sigma_e}{g} \right)^{1/m} \tag{3}$$

Here, α denotes the parameter related to plastic compressibility, $\dot{\epsilon}_0$ and m stand for, respectively, the reference strain rate and rate hardening exponent. The hardness function $g(\epsilon_p)$ is given as

$$g(\epsilon_p) = \sigma_0 \begin{cases} 1 + h_1 \epsilon_p, & \epsilon_p < \epsilon_1 \\ 1 + h_1 \epsilon_1 + h_2 (\epsilon_p - \epsilon_1), & \epsilon_1 < \epsilon_p < \epsilon_2 \\ 1 + h_1 \epsilon_1 + h_2 (\epsilon_2 - \epsilon_1) + h_3 (\epsilon_p - \epsilon_2), & \epsilon_p > \epsilon_2 \end{cases} \tag{4}$$

here, σ_0 indicates a reference stress. Also, the effective stress σ_e in equation (3) is described as

$$\sigma_e^2 = \frac{3}{2} \tau : p = \frac{3}{2} \left[\tau : \tau - \alpha (tr(\tau))^2 \right] \tag{5}$$

When the value of α is 1/3, the present constitutive equation becomes that of plastically incompressible Mises solid with isotropic hardening.

2.2 Definition of the Problem

Numerical results are generated here for two different materials, B (bilinear hardening) and E (trilinear hardening-softening-hardening)¹⁴. The hardness function plots of these materials are presented in Fig. 1 using equation 4. The values of h_1 and ϵ_1 are same for both the materials and those are 24 and 0.085, respectively. For material B, h_2 and h_3 are same and it is 5.0 while these values are -3.90 and 15.0, respectively for material E. The other fixed parameters are $E/\sigma_0 = 100$, $\dot{\epsilon}_0 = 1$ and $m = 0.02$.

A semicircular geometry (as shown in Fig. 2(a)) with radius $R_0 = 2.0$ in arbitrary units is considered for simulation. In the geometry, a notch of initial radius, b_0 in the same units is also there and the centre of the notch is at the origin of the reference system, Fig. 2(b).

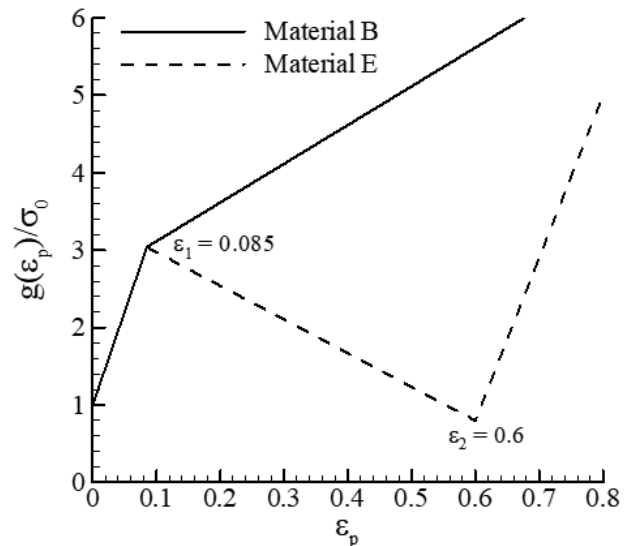


Figure 1. Hardness function plot of materials B and E¹⁴.

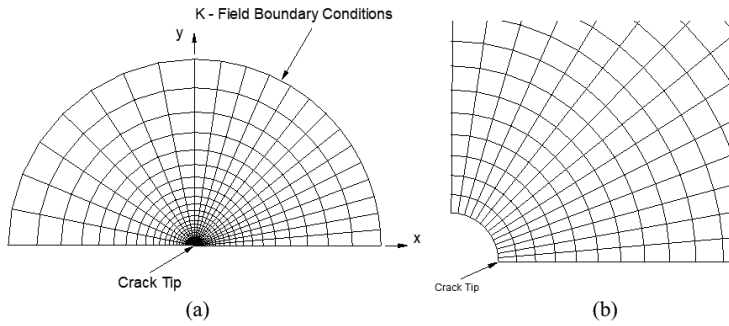


Figure 2. Finite element mesh for the analysis; (a) full mesh and (b) near-tip mesh.

2.3 Method of Analysis

For generating mesh, we consider quadrilateral elements each of which further comprises of four triangular elements (with constant strain) arranged in a crossed triangle configuration. Where there is finite strain, for reproducing localised deformation, such crossed elements with appropriate aspect ratio as well as orientation are widely used¹⁶. On the outside boundary of the geometry, K_I field displacements are prescribed.

$$\dot{u}_1 = \frac{2(1+\nu)\dot{K}_I}{E} \sqrt{\frac{R}{2\pi}} \cos\left(\frac{\theta}{2}\right) \left[1 - 2\nu + \sin^2\left(\frac{\theta}{2}\right)\right] \quad (6)$$

$$\dot{u}_2 = \frac{2(1+\nu)\dot{K}_I}{E} \sqrt{\frac{R}{2\pi}} \sin\left(\frac{\theta}{2}\right) \left[2 - 2\nu + \cos^2\left(\frac{\theta}{2}\right)\right] \quad (7)$$

where, K_I is the mode I stress intensity factor. The analogous value of applied J i. e. J_{app} , during SSY, is given by Rice¹⁷ as

$$J_{app} = K_I^2(1-\nu^2)/E \quad (8)$$

For the present simulation, $(K_I)_{max}/K_{ref} = 2$ and $(K_I)_{min}/K_{ref} = 0$ with $K_{ref} = \sigma_0\sqrt{1000b_0}$. Triangular shape waveform has been chosen for all fatigue loading cycles and there are total ten load cycles used in the simulation. In this finite deformation finite element formulation, for the field equations, we use convected coordinate based on Lagrangian formulation^{14-15, 18-19}. A constant normalised loading rate of $\dot{K}_I/\sigma_0\dot{\epsilon}_0\sqrt{b_0}$ is found to be approximately 32 with stress intensity factor rate \dot{K}_I is $1 \text{ MPa}\sqrt{\text{ms}}^{-1}$. Linear increments are employed to calculate the deformation history with time step size of 0.0002. For the constitutive update, a rate tangent modulus method is adopted²⁰. Figure 2 represents the present mesh density. This study focuses exclusively on the crack growth simulation due to the fact that the crack-tip blunting effects are most dominant¹⁵.

3. NUMERICAL RESULTS

Mesh convergence study was carried out with 24×53 , 24×63 , and 24×73 rectangular elements without any special element at crack-tip. Plastic strain contours at the tip have been compared and the strain contours with respect to 24×63 and 24×73 elements are almost identical as compared to 24×53 . For other mesh densities also, plastic strain solutions were generated; apart from the initial coarse mesh,

the required solutions were quite steady representing too small differences at higher mesh densities. Comparing the solution accuracy as well as time required for the solution, the final mesh density has been fixed at 24×63 rectangular elements with 1598 nodes. With sufficiently fine mesh at the crack-tip, the radial length of a finite element just next to the crack-tip is roughly $b_0/10$.

The accuracy of the present numerical results can be further checked by noting the similarity of the near-tip stress distributions for a propagating crack of Liu and Drugan²¹ under monotonic load. Liu and Drugan used linear elastic - perfectly plastic material model with E as 200 GPa, ν as 0.5 and yield stress as 1.173 GPa. Using identical conditions, the finite element simulation was run with the present code and subsequently the normal and shear stresses are plotted in Fig. 3. The maximum σ_{xx} and σ_{yy} values (approximately 1.6 and 2.6, respectively) are almost matching with those of Liu and Drugan. The pattern of the stress distribution is too almost identical. The minute discrepancy may be owing to dissimilar finite elements. In this work, we employed crossed quadrilateral elements but Liu and Drugan considered usual quadrilateral elements in their analysis. Therefore, the results in Fig. 3 provide us enough confidence to move on with more investigations.

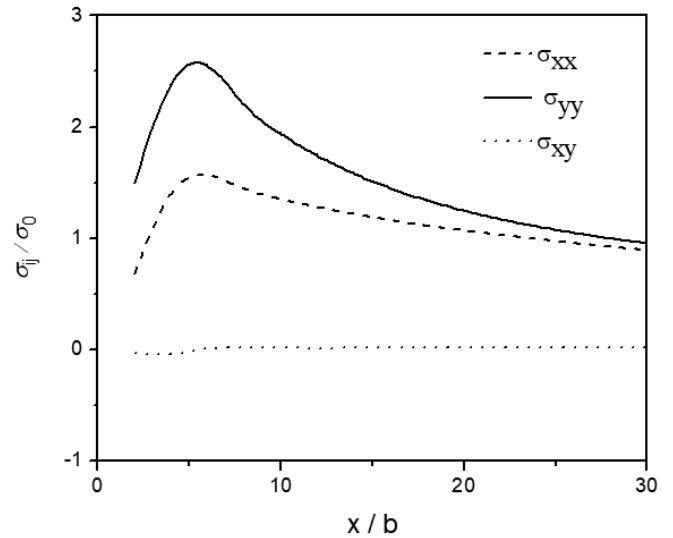


Figure 3. Distribution of normal and shear stresses ahead of a propagating crack (with $\Delta a = 0.0086(K_I/\sigma_0)^2$) in a linear elastic - perfectly plastic material.

3.1 Fatigue crack growth

Even though there are various techniques for crack growth simulation, like node release scheme, cohesive zone model etc., the present crack growth modelling strategy is based on crack-tip blunting model¹⁵. According to this model, in a single complete load cycle, the tip of a crack blunts when the load increases from initial to maximum value and the crack-tip re-sharpens during the period of the unloading. The crack growth comes solely by the crack-tip plasticity only.

The crack growth ($\Delta a/b_0$) against time (t/t_0) for the materials B and E is presented in Figs. 4-5. The normalisation time t_0 is defined by, $t_0 = \epsilon_0/\dot{\epsilon}_0$, where $\epsilon_0 (= \sigma_0/E)$ is the

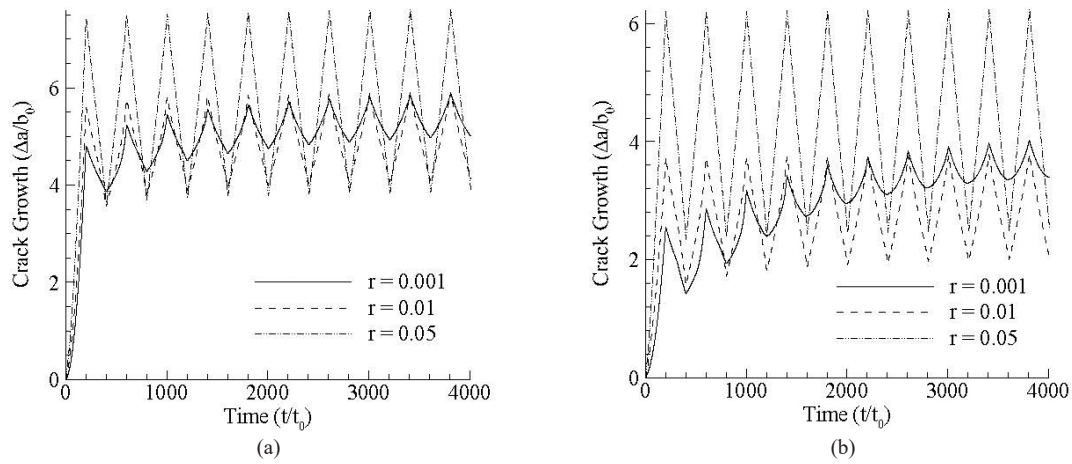


Figure 4. Normalised crack growth versus normalised time near the crack-tip, material B (a) $\alpha = 1/3$ (plastically incompressible) and (b) $\alpha = 0.28$ (plastically compressible).

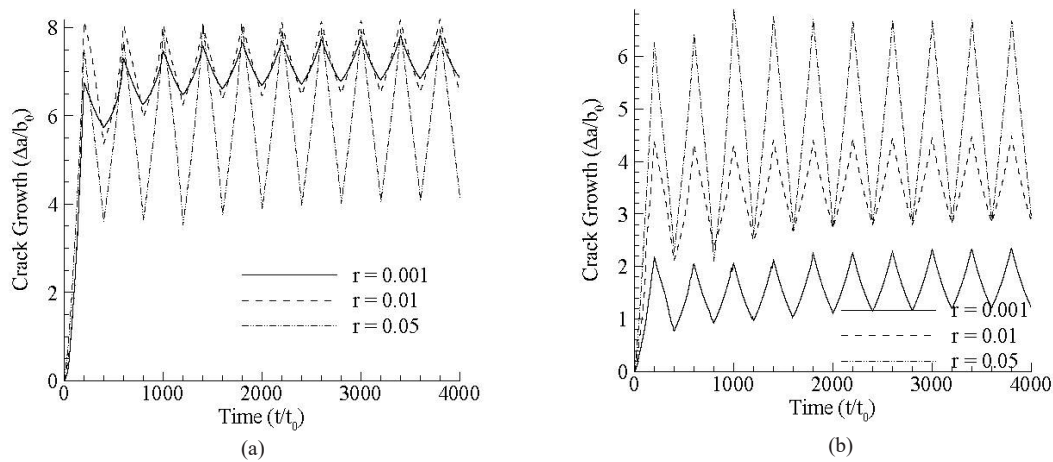


Figure 5. Normalised crack growth versus normalised time near the crack-tip, material E (a) $\alpha = 1/3$ and (b) $\alpha = 0.28$.

strain at yield point and its value is 0.01. The resulting crack growth corresponding to each radius may be obtained by joining the valley points of the crack growth curve through line/ curve. For both the materials the maximum crack growth takes place during the first cycle and then it rises slowly. Crack growth is very much influenced by plastic compressibility and tip radius. Because of plastic compressibility, there is reduction in the resulting crack growth for both the materials. In material B for minimum tip radius (i. e. 0.001) the resulting crack growth is maximum due to the stress concentration effect as would be shown later. In Fig. 4(b), the crack growth corresponding to radius 0.05 is slightly more as compared to that of radius 0.01 and it may be because of the variation in near-tip strain localisation pattern for plastically compressible solids as discussed in section 3.2. In material E when it is plastically incompressible, for the smallest tip radius, the crack growth is again highest and also among all the cases Fig. 5(a) shows the greatest amount of crack-tip extension due to the material softening. Conversely, for material E when $\alpha = 0.28$, just opposite trend occurs, i. e. for the least crack-tip radius, the resulting crack growth is also least and crack growth is increased with increase in crack-tip radius. This is very unusual and will be cleared from section 3.2. The rate of crack growth da/dN is maximum during the

1st cycle and then gradually reducing. Also, because of plastic compressibility, da/dN during the first loading cycle is highest for the maximum crack-tip radius size and the rate is least for the smallest tip radius. The plastic compressibility together with material softening diminishes the amount of growth significantly. The present FCG for plastically incompressible solids shows the similar trend (in a qualitative way) when we compare our results with those of Rozumek⁷, Toribio and Kharin²², Borges²³, *et al.*

3.2 Effect of Initial Crack-tip Radius Size on Deformation and Near-tip Fields

Now, we demonstrate the development of near-tip contours of accumulated plastic strain ϵ_p and hydrostatic stress (σ_h / σ_0) together with the crack-tip deformation pattern with respect to the number of load cycles for materials B and E, Figs. 6 – 13. Here, main focus is to correlate the distribution of ϵ_p and (σ_h / σ_0) with the crack-tip shape and subsequently the FCG. Only plastically compressible solids have been considered for illustration. While considering material B, Figs. 6 and 7 represent the near-tip distribution of ϵ_p and (σ_h / σ_0), respectively, corresponding to crack-tip radius of 0.001 and on the other hand Figs. 8 - 9 represent the similar

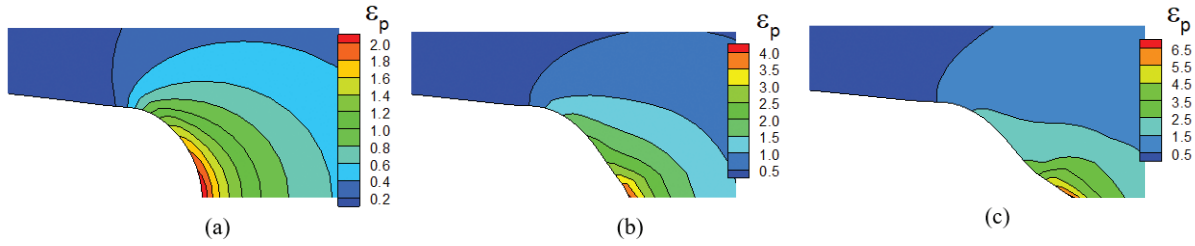


Figure 6. Distribution of ϵ_p for material B, $\alpha = 0.28$, and $b_0 = 0.001$; after (a) 1st cycle, (b) 3rd cycle and (c) 10th cycle.

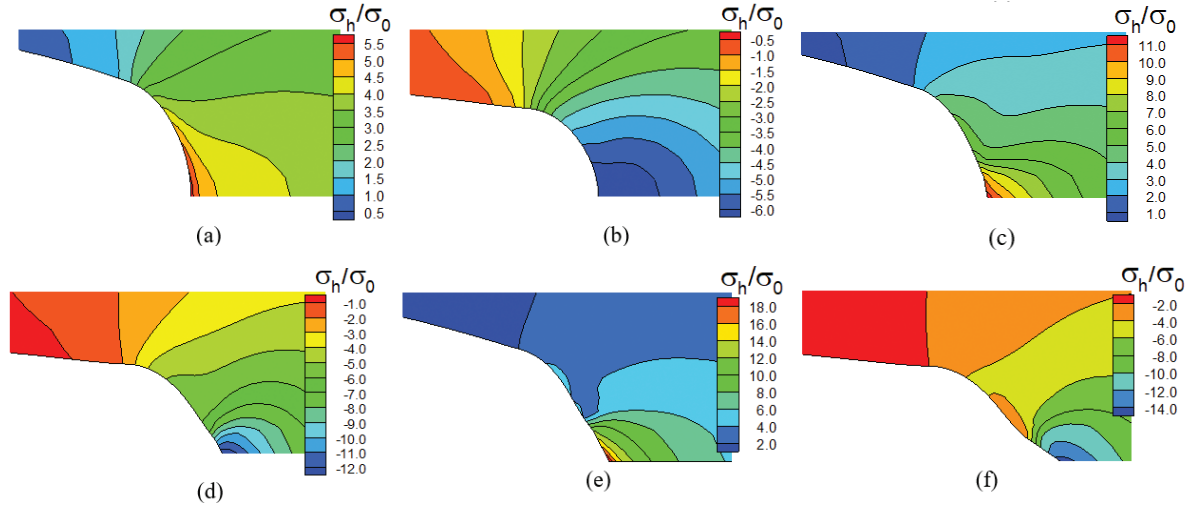


Figure 7. Distribution of (σ_h / σ_0) for material B, $\alpha = 0.28$, and $b_0 = 0.001$; after (a) 1st cycle loading phase, (b) 1st cycle, (c) 3rd cycle loading phase, (d) 3rd cycle, (e) 10th cycle loading phase, and (f) 10th cycle.

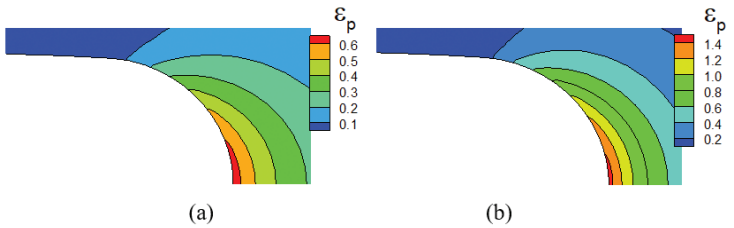


Figure 8. Distribution of ϵ_p for material B, $\alpha = 0.28$, and $b_0 = 0.01$; after (a) 1st cycle and (b) 10th cycle.

distributions corresponding to the tip radius of 0.01. The nature of crack-tip blunting is dissimilar for both the crack-tip radii. In Fig. 6, as the number of load cycle increases the accumulated plastic strain concentrates more on the tip (rather than on the crack surface) with greater magnitude of the strain and the tip is becoming sharper. The near-tip distribution of the equivalent stress has also been noted and it is similar to the plastic strain distribution and for brevity these are not plotted; the corresponding normalised equivalent stress values (σ_e / σ_0)

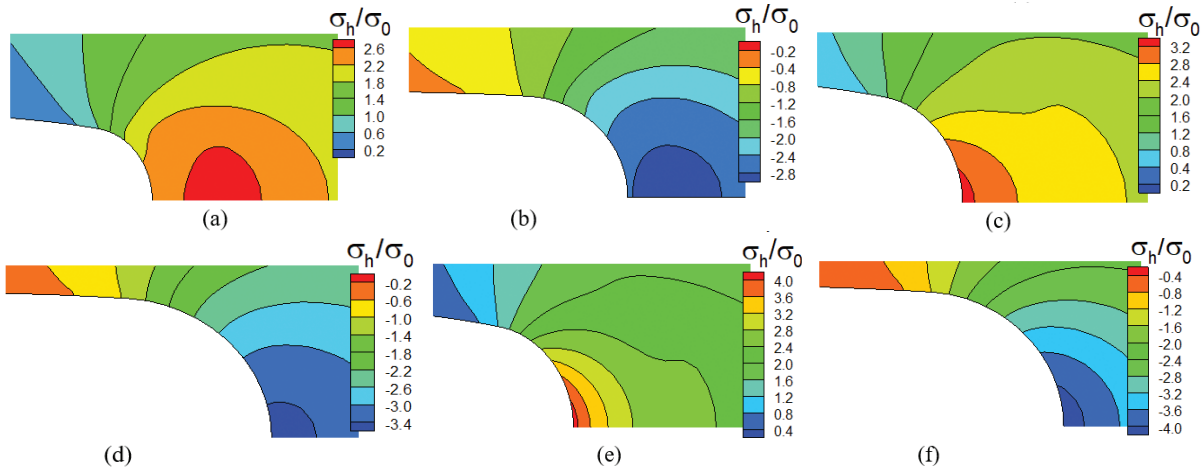


Figure 9. Distribution of (σ_h / σ_0) for material B, $\alpha = 0.28$, and $b_0 = 0.01$; after (a) 1st cycle loading phase, (b) 1st cycle, (c) 3rd cycle loading phase, (d) 3rd cycle, (e) 10th cycle loading phase, and (f) 10th cycle.

after 1st, 2nd and the 3rd cycle are 12, 22 and 34, respectively. In plastically compressible materials, the hydrostatic stress is supposed to play a vital role in localisation of shear band and its propagation. The hydrostatic stress distribution for both $K_I \rightarrow (K_I)_{\max}$ and $K_I \rightarrow (K_I)_{\min}$ of 1st, 3rd and 10th cycle corresponding to the tip radius 0.001 is plotted in Fig. 7. At the end of unloading, the near-tip hydrostatic stress is compressive in nature as expected. As the number of load cycle increases, the positive and negative maximum stress values are concentrated more on the crack-tip like the ϵ_p distribution. For the tip radius of 0.01, on the other hand, the ϵ_p is distributed on the crack surface throughout the loading history though there is increase in the maximum value of the plastic strain with the number of load cycles, Fig. 8. Here, initially, the contour of the peak (σ_h / σ_0) is slightly away from the tip and with the increase in the number of load cycle, the peak stress contour becomes attached to the crack surface more with higher compressive stress. Further, Figs. 7 and 9 reveal that the compressive hydrostatic stress is more for tip radius 0.001 as compared to that of corresponding tip radius of 0.01 for unloading phase of any cycle and this may be explanation for making the crack-tip sharper during the unloading and more FCG during the subsequent reloading.

We next describe the crack-tip contours of ϵ_p and (σ_h / σ_0) for material E in Figs. 10 – 13 as the fatigue load cycle increases. In material E, with tip radius of 0.001, in the 1st cycle itself, the crack-tip becomes very blunt and this shape is continued up to the 10th cycle although the maximum plastic strain value increases from 1.5 to 1.9, Fig. 10. The deformed crack surface is nearly vertical. The shape of the maximum plastic strain contour is slightly changed with loading; initially the spread of the contour is nearly on the whole crack-tip surface but with increase in the load cycle, the maximum plastic strain contour is concentrated at the corner of the crack surface. Similarly, with increase in the load cycles, the maximum hydrostatic stress contour (with more compressive stress magnitude) is concentrated in a circular fashion at the corner. Here, in any cycle, the negative maximum hydrostatic stress value is less in comparison with the same of the material B because of the material softening, Fig. 11. For the crack-tip radius of 0.01, in contrast, the ϵ_p is distributed on the tip throughout the loading history and also there is increase in the maximum plastic strain value, Fig. 12. Both positive and negative peak hydrostatic stress contours are attached at the crack-tip though the maximum compressive stress value is increasing with load cycle. In contrast to the behaviour of material B, as the location of maximum negative hydrostatic stress for the crack-tip radius 0.01 is at the tip now, the sharpness during the unloading of any load cycle is more and this causes the crack growth more. Thus, one may conclude that when the initial crack-tip radius is lowest, the rate of FCG is found to be highest for hardening material; but in sharp disparity, when the material (plastically compressible) exhibits strain softening, the FCG rate is found to be dependent on the instantaneous crack-tip radius.

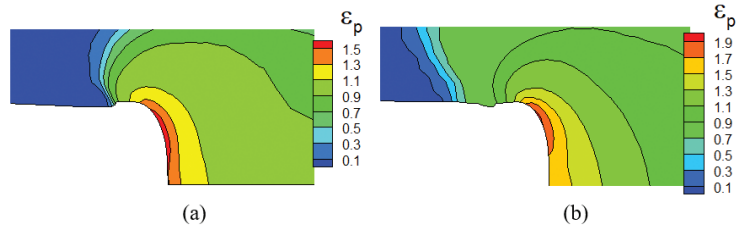


Figure 10. Distribution of ϵ_p for material E, $\alpha = 0.28$, and $b_0 = 0.001$; after a) 1st cycle, b) 10th cycle.

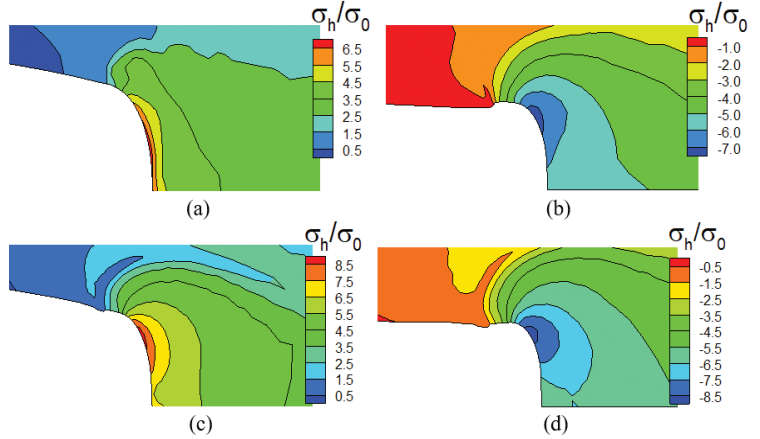


Figure 11. Distribution of (σ_h / σ_0) for material E, $\alpha = 0.28$, and $b_0 = 0.001$; after (a) 1st cycle loading, (b) 1st cycle unloading, (c) 10th cycle loading, and (d) 10th cycle unloading.

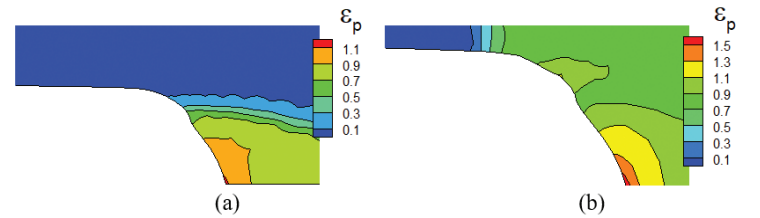


Figure 12. Distribution of ϵ_p for material E, $\alpha = 0.28$, and $b_0 = 0.01$; after (a) 1st cycle and (b) 10th cycle.

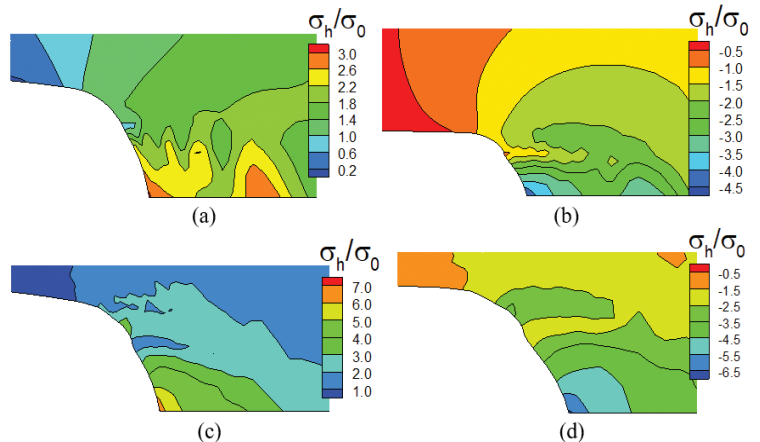


Figure 13. Distribution of (σ_h / σ_0) for material E, $\alpha = 0.28$, and $b_0 = 0.01$; after (a) 1st cycle loading, (b) 1st cycle unloading, (c) 10th cycle loading, and (d) 10th cycle unloading.

4. CONCLUSIONS

The results of the FCG simulations and near-tip stress-strain fields on different crack-tip radii for plastically compressible bilinear hardening and trilinear hardening-softening-hardening materials allow us to draw the following concluding remarks:

- (i) The crack-tip radius strongly influences the crack-tip deformation, fields and the FCG.
- (ii) For the hardening-hardening material, the amount of FCG is found to be maximum with smallest crack-tip radius though the FCG variation is dissimilar in plastically compressible and incompressible solids.
- (iii) In presence of strain softening in plastically compressible solid, the FCG, however, is dependent on the instantaneous crack-tip radius and not on the initial crack-tip radius.
- (iv) The plastic compressibility significantly reduces the FCG.

REFERENCES

1. McMeeking R.M. Finite deformation analysis of crack tip opening in elastic-plastic materials and implications for fracture. *J. Mech. Phys. Solids*, 1977, **25**, 357–381. doi:10.1016/0022-5096(77)90003-5
2. Ishikawa, M.; Narisawa, I. & Ogawa, H. Criterion for craze nucleation in polycarbonate. *J. Polym. Sci. Polym. Phys. Ed*, 1977, **15**, 1791-1804. doi:10.1002/pol.1977.180151009
3. Narisawa, I. & Yee, A. F. Cralabelled and fracture in polymers. structure and properties of polymers. *Mater. Sci. Technol., A Comprehensive Treatment*, 1993, **12**, 699-765.
4. Nishida, T.; Hanaki, Y.& Pezzotti G. Effect of notch root radius on the fracture toughness of a fine grained alumina. *J. Am. Ceram. Soc.*, 1994, **77**, 606–8. doi:10.1111/j.1151-2916.1994.tb07038.x
5. Damani, R.; Gstrein, R. & Danzer, R. Critical notch-root radius effect in SENB-S fracture toughness testing. *J. Eur. Ceram. Soc.*, 1996, **16**(7), 695–702. doi:10.1016/0955-2219(95)00197-2
6. Picard, D.; Leguillon, C. & Putot, C. A method to estimate the influence of the notch-root radius on the fracture toughness measurement of ceramics. *J. Eur. Ceram. Soc.*, 2006, **26**, 1421–1427. doi:10.1016/j.jeurceramsoc.2005.02.016
7. Rozumek, D.; Macha, E.; Lazzarin, P. & Meneghetti, G. Influence of notch (Tip) radius on fatigue crack growth rate. *J. Theor. Appl. Mech.*, 2006, **44**(1), 127 – 137.
8. Yanase, K. & Endu, M. Analysis of notch effect in fatigue. *J. ASTM Int.*, 2012, **9**(4), 1-13. doi:10.1520/JAI103944
9. Mohan, N. Extracting material response from simple mechanical tests on hardening-softening-hardening viscoplastic solids, California Institute of Technology Pasadena, California, 2014. (*PhD Thesis*).
10. Hutchens, S.B.; Hall L.J. & Greer J.R. In situ mechanical testing reveals periodic buckle nucleation and propagation in carbon nanotube bundles. *Adv. Funct. Mater.*, 2010, **20**, 2338–2346. doi:10.1002/adfm.201000305
11. Hutchens, S.B.; Needleman, A. & Greer, J.R. Analysis of uniaxial compression of vertically aligned carbon nanotubes. *J. Mech. Phys. Solids*, 2011, **59**, 2227-2237. doi:10.1016/j.jmps.2011.05.002
12. Deshpande, V.A. & Fleck, N.A. Isotropic constitutive models for metallic foams. *J. Mech. Phys. Solids*, 2000, **48**, 1253–1283. doi:10.1016/S0022-5096(99)00082-4
13. Tanwongwan, W. & Carmai, J. Finite element modelling of titanium foam behavior for dental application. In Proceedings of World Congress on Engineering 2011, London.
14. Mohan, N.; Cheng, J.; Greer, J.R. & Needleman, A. Uniaxial tension of a class of compressible solids with plastic non-normality. *J. Appl. Mech.*, 2013, **80**(4), 1-8. doi:10.1115/1.4024179
15. Singh, S. and Khan, D. On fatigue crack growth in plastically compressible hardening and hardening-softening-hardening solids using crack tip blunting. *Int. J. Fract.*, 2018, **213**, 139 – 155. doi:10.1007/s10704-018-0310-y
16. Wu, P. D. and Van der Giessen, E. Computational aspects of localized deformations in amorphous glassy polymers. *Eur. J. Mech. A/ Solids*. 1996, **15**(5), 799-823
17. Rice, J. R. A path independent integral and the approximate analysis of strain concentration by notches and cracks. *J. Appl. Mech.*, 1968, **90**, 379 – 386. doi:10.1115/1.3601206
18. Needleman, A.; Hutchens, S.B.; Mohan, N. & Greer, J. R. Deformation of plastically compressible hardening-softening-hardening solids. *Acta Mech. Sin.*, 2012, **28**, 1115–1124. doi:10.1007/s10409-012-0117-4
19. Khan, D.; Singh, S. & Needleman, A. Finite deformation analysis of crack tip fields in plastically compressible hardening-softening-hardening solids. *Acta Mech. Sin.*, 2017, **33**(1), 148-158. doi:10.1007/s10409-016-0614-y
20. Peirce, D.; Shih, C.F. & Needleman, A. A tangent modulus method for rate dependent solids. *Comput. Struct.*, 1984, **18**(5), 875-887. doi:10.1016/0045-7949(84)90033-6
21. Liu, N. & Drugan, W., J. Finite element solution for crack growth in incompressible elastic plastic solids with various yielding extents and loadings: Detailed comparisons with analytical solutions. *Int. J. Fract.*, 1993, **59**, 265-289. doi:10.1007/BF00012365
22. Toribio, T. & Kharin, V. Finite-deformation analysis of the crack-tip fields under cyclic loading, *Int. J. Solids Struct.*, 2009, **46**(9), 1937-1952. doi:10.1016/j.ijsolstr.2009.01.006
23. Borges, M.; Caldas, M.; Antunes, F.; Branco, R. & Prates, P. fatigue crack growth from notches: a numerical analysis, *Appl. Sci.*, 2020, **10**, 4174. doi:10.3390/app10124174

CONTRIBUTORS

Dr S. Singh did his PhD in Mechanical Engineering from IIT (BHU) Varanasi and presently working as an Assistant Professor in Uttaranchal University, Dehradun. His research interests include finite element method, plasticity, fracture mechanics, plastically compressible materials etc. He has published a number of research papers in international journals and conferences.

In the current study, he has generated all the data from the finite element simulation, plotted the graphs and written the manuscript.

Dr D. Khan received his PhD from Indian Institute of Technology Kharagpur. Currently, he is working as an Associate Professor in the Department of Mechanical Engineering, IIT (BHU) Varanasi. He has published several research papers in international journals and conferences. His areas of research are solid mechanics, fracture mechanics, finite deformation plasticity, finite element method etc.

In the current study, he has checked and corrected the manuscript. All the simulation studies mentioned in the paper was suggested by him.